UCT943, a next generation *Plasmodium falciparum* PI4K inhibitor preclinical candidate for the treatment of malaria

Christel Brunschwig[a], Nina Lawrence[a], Dale Taylor[a], Efrem Abay[a], Mathew Njoroge[a], Gregory S. Basarab[a], Claire Le Manach[b], Tanya Paquet[b], Diego Gonzàlez Cabrera[b], Aloysius T. Nchinda[b], Carmen de Kock[a], Lubbe Wiesner[c], Paolo Denti[c], David Waterson[d], Benjamin Blasco[d], Didier Leroy[d], Michael J. Witty[d], Cristina Donini[d], James Duffy[d], Sergio Wittlin[e,f], Karen L. White[g], Susan A. Charman[g], Maria Belén Jiménez-Díaz[h], Iñigo Angulo-Barturen[h], Esperanza Herreros[h], Francisco Javier Gamo[h], Rosemary Rochford[i], Dalu Mancama[j], Theresa L. Coetzer[k], Mariëtte E. van der Watt[l], Janette Reader[l], Lyn-Marie Birkholtz[l], Kennan C. Marsh[m], Suresh M. Solapure[n], Manu Vanaerschot[o], David A. Fidock[o,p], Paul V. Fish[q], Peter Siegl[r], Dennis A. Smith[s], Grennady Wirjanata[t], Rintis Noviyanti[u], Ric N. Price[t,v], Jutta Marfurt[t], Kigbafori D. Silue[w], Leslie J. Street[b], Kelly Chibale[b,x,y #]

[a] Drug Discovery and Development Centre (H3D), Division of Clinical Pharmacology, Department of Medicine, University of Cape Town, Observatory, 7925, South Africa

[b] Drug Discovery and Development Centre (H3D), Department of Chemistry, University of Cape Town, Rondebosch 7701, South Africa

[c] Division of Clinical Pharmacology, Department of Medicine, University of Cape Town, Observatory, 7925, South Africa

[d] Medicines for Malaria Venture, ICC, Route de Pré -Bois 20, P.O. Box 1826, 1215 Geneva, Switzerland

[e] Swiss Tropical and Public Health Institute, Socinstrasse 57, 4002 Basel, Switzerland

[f] University of Basel, 4003 Basel, Switzerland

[g] Centre for Drug Candidate Optimisation, Monash University, 381 Royal Parade, Parkville, Melbourne, Victoria 3052 Australia

[h] GlaxoSmithKline, Tres Cantos Medicines Development Campus, Severo Ochoa, 2, 28760 Tres Cantos, Madrid, Spain

[i] Departments of Immunology and Microbiology, University of Colorado, Denver, Aurora, CO, United States

[j] Biosciences, Council for Scientific and Industrial Research, PO Box 395, Pretoria 0001, South Africa

[k] Plasmodium Molecular Research Unit, Wits Research Institute for Malaria, Department of Molecular Medicine and Haematology, School of Pathology, Faculty of Health Sciences, University of the Witwatersrand and National Health Laboratory Service, Johannesburg 2193, South Africa

[l] Department of Biochemistry, Institute for Sustainable Malaria Control and South African Medical Research Council Collaborating Centre for Malaria Research, University of Pretoria, Private Bag x20, Hatfield, Pretoria 0028, South Africa

[m] AbbVie, 1 North Waukegan Road, North Chicago, Il 60064-6104, United States

[n] Nagarjuna Gardens, 60 Feet Road, Sahakaranagar, Bangalore 560092, India

[o] Department of Microbiology and Immunology, Columbia University Medical Center, New York, New York 10032, United States

[p] Division of Infectious Diseases, Department of Medicine, Columbia University Medical Center, New York, New York 10032, United States

[q] Alzheimer's Research UK UCL Drug Discovery Institute, Faculty of Brain Sciences, University College London, Gower Street, London, United Kingdom

[r] Siegl Pharma Consulting LLC, Blue Bell, PA, United States

[s] 4 the Maltings, Walmer, Kent, United Kingdom

[t] Global and Tropical Health Division, Menzies School of Health Research, Charles Darwin University, PO Box 41096, Casuarina, NT 0811, Darwin, Australia

[u] Eijkman Institute for Molecular Biology, Jalan Diponegoro 69, 10430 Jakarta, Indonesia

[v] Centre for Tropical Medicine and Global Health, Nuffield Department of Clinical Medicine, University of Oxford, United Kingdom

[w] Centre Suisse de Recherches Scientifiques en Côte d'Ivoire, Km17 Route de Dabou, Adipodoumé, 01 BP 1303 Abidjan, Côte d'Ivoire

[x] Institute of Infectious Disease and Molecular Medicine, University of Cape Town, Rondebosch 7701, South Africa

[y] South African Medical Research Council Drug Discovery and Development Research Unit, Department of Chemistry, University of Cape Town, Rondebosch 7701, South Africa

#corresponding author: kelly.chibale@uct.ac.za

Abstract

The 2-aminopyridine MMV048 was the first drug candidate inhibiting *Plasmodium* phosphatidylinositol 4-kinase (PI4K), a novel drug target for malaria, to enter clinical development. In an effort to identify the next generation of PI4K inhibitors, the series was optimized to improve properties such as solubility and antiplasmodial potency across the parasite lifecycle, leading to the 2-aminopyrazine UCT943. The compound displayed higher

asexual blood stage, transmission-blocking, and liver stage activity than MMV048 and was more potent against resistant *P. falciparum* and *P. vivax* clinical isolates. Excellent *in vitro* antiplasmodial activity translated into high efficacy in *P. berghei* and humanized *P. falciparum* NOD-*scid IL-2Rγ*^{null} mouse models. The high passive permeability and high aqueous solubility of UCT943, combined with low to moderate *in vitro* intrinsic clearance, resulted in sustained exposure and high bioavailability in preclinical species. In addition, the predicted human dose for a curative single administration using monkey and dog pharmacokinetics was low, ranging from 50 to 80 mg. As a next generation *Plasmodium* PI4K inhibitor, the combined preclinical data suggest that UCT943 has the potential to form part of a single-exposure radical cure and prophylaxis (SERCaP) to treat, prevent and block the transmission of malaria.

1 INTRODUCTION

Malaria, an infectious disease transmitted to people through the bite of female *Anopheles* mosquitoes infected with *Plasmodium falciparum* (*Pf*) or *Plasmodium vivax* (*Pv*), still afflicts millions of people, with almost 90% of cases on the African continent. Even though the number of malaria cases has fallen globally from an estimated 237 million cases in 2010 to 216 million cases in 2016, malaria still causes 445 000 deaths per year, 99% of which are due to *Pf* in Africa (1). Parasite resistance against currently recommended artemisinin-based combination therapies (2, 3) is a concern, and antimalarial drugs with a novel mode of action are urgently needed. We previously reported the identification of the 2-aminopyridine compound MMV390048 (also known as MMV048), which is efficacious *in vivo* against all measurable *Plasmodium* life cycle stages, except hypnozoites (4). MMV048

acts through the inhibition of *Plasmodium* phosphatidylinositol 4-kinase (PI4K) and is the first and sole agent with this mode of action that has entered clinical development. PI4K was reported as a target for *Plasmodium* in 2013 with inhibition by other compound classes (5). The low aqueous solubility associated with MMV048 in biorelevant media was identified as one of the issues to address in the next generation of PI4K inhibitors along with improved potency. Towards this goal, a scaffold change from the 2-aminopyridine to the 2-aminopyrazine core with concomitant introduction of aqueous solubilizing groups delivered analogues with a better developability profile with respect to improved physicochemical properties, as well as a significant improvement in potency across the parasite lifecycle . Improved aqueous solubility was optimally achieved through the incorporation of a piperazinylamide group on the phenyl ring at the 5-position of the 2-aminopyrazine scaffold, leading to UCT943 (Figure 1). This compound, among other attributes, showed potent *in vitro* activity against multiple stages of the parasite lifecycle and excellent *in vivo* efficacy in the *Plasmodium berghei* and *P. falciparum* NSG (NOD-*scid IL-2Rγ*^{null}*)* mouse models (6). In order to assess the potential of UCT943 as a follow-on compound to MMV048 and a preclinical antimalarial candidate, physicochemical, parasitological, and pharmacological profiling was undertaken. Furthermore, extensive drug metabolism and pharmacokinetics (DMPK) profiling was carried out in order to facilitate the prediction of human pharmacokinetic (PK) parameters and the efficacious single dose in humans. The results are reported herein.

2 MATERIAL AND METHODS

2.1 Chemistry

UCT943 was synthesized in seven steps from commercially available 2-aminopyrazine, as previously described (6).

2.2 *In vitro* antiplasmodial activity

2.2.1 Asexual blood stage assays

2.2.1.1 Cross-resistance against field isolates

UCT943 was tested using the [^{3}H]-hypoxanthine incorporation assay (7, 8) against a panel of drug sensitive and drug resistant *P. falciparum* strains (Supplementary Material Table S1), as well as against a panel of resistant *P. falciparum* clones generated in the laboratory of Prof David Fidock (Columbia University, USA) (Supplementary Material Table S2).

2.2.1.2 In vitro P. falciparum resistance generation to UCT943 and pi4k gene sequencing

The generation of UCT943-resistant *Pf* clones was performed as described elsewhere (4) (see Supplementary Material Table S4).

2.2.1.3 Ex vivo assay against resistant P. falciparum clinical isolates from Côte d'Ivoire

Drug susceptibility of *P. falciparum* isolates from Côte d'Ivoire, West Africa was measured using incorporation of SYBR® Green into the parasite's DNA as described before (9). The drug plates contained 10 serial concentrations of the antimalarials, with maximum concentration of 1170 nM for UCT943.

2.2.1.4 Ex Vivo schizont maturation drug susceptibility assay against P. vivax and P. falciparum clinical isolates

Drug susceptibility of *P. vivax* and *P. falciparum* isolates from Papua, Indonesia was measured using a modified schizont maturation assay as described previously (9). The drug plates contained 11 serial concentrations of the antimalarials, with maximum

concentrations of 2993 nM for chloroquine, 1029 nM for piperaquine, 338 nM for mefloquine, 49 nM for artesunate, and 297 nM for UCT943.

2.2.2 Liver stage assays

2.2.2.1 P. berghei liver stage assay

Plasmodium berghei luciferase sporozoites were obtained by dissection of infected *Anopheles stephensi* mosquito salivary glands. The sporozoite invasion assay was performed as described in (6) using the rodent parasite *P. berghei* that is able to infect human hepatocarcinoma HepG2-A16-CD81EGFP cells (10, 11).

2.2.2.2 P. cynomolgi liver stage assay

Primary rhesus hepatocytes were infected *in vitro* with *P. cynomolgi* sporozoites and the drug assays performed as previously reported by Zeeman *et al.* (12).

2.2.2.3 P. vivax liver stage assay

The *P. vivax* liver stage assay was implemented in human hepatocytes, infected *in vitro* with *P. vivax* sporozoites, according to the protocol described in (13).

2.2.3 Gametocyte assays

In vitro gametocytocidal activity was determined using luciferase reporter lines specifically enabling screening against early stage gametocytes (>90% stage I-III) and late stage gametocytes (>95% stage IV-V) as per Reader *et al*. (14). Methylene blue (5 µM) and MMV048 (5 µM) were routinely included as controls.

2.2.4 P. falciparum Dual Gamete Formation Assay (Pf DGFA)

Transmission-blocking activity of UCT943 was assessed in the DGFA, which utilizes a dual read-out that individually and simultaneously reports on the functional viability of male and female mature stage V gametocytes, as per Ruecker *et al.* (15).

159 ### 2.3 Physicochemical properties

160 The pKa of UCT943 was determined by potentiometric titration as described previously (16).
161 Solubility was measured after 24 h incubation of solid material with media at 37°C with
162 residual solids checked by XRPD. Media included five pH buffers (pH 2.0, 4.0, 6.0, 8.0, and
163 10.0) and three bio-relevant media: Simulated Gastric Fluid (SGF) pH 1.8, Fasted State
164 Simulated Intestinal Fluid (FaSSIF) pH 6.5 and Fed State Simulated Intestinal Fluid (FeSSIF)
165 pH 5.0. Analyses were done by High Performance Liquid Chromatography (HPLC) (Waters
166 Xbridge C18, 150 × 4.6 mm, 3 µm) at 40°C with a mobile phase of 0.1% trifluoroacetic acid
167 (TFA) in water and 0.1% TFA in acetonitrile with UV detection (220 nm, reference 500 nm).

168 ### 2.4 *In vitro* metabolism studies

169 Metabolic stability of UCT943 (1 µM) was assessed in human, dog, rat, and mouse liver
170 microsomes using a 5-point assay and LC-MS/MS as described in (17). Metabolic stability (1
171 µM) was also evaluated with cryopreserved hepatocytes from the same species (1 x 10^6
172 viable cells/mL), as described in (18). Hepatic extraction ratio's (E_H) were calculated using
173 physiological based scaling factors as previously described (19).
174 Binding to plasma proteins and microsomal proteins (0.5 mg/mL) was determined by
175 ultracentrifugation with LC-MS analysis as described in (20) and (17), respectively.
176 Permeability was determined across Caco-2 monolayers in both apical to basolateral and
177 basolateral to apical directions using pH 7.4 in both apical and basolateral chambers, as
178 reported in (9).
179 Cytochrome P450 (CYP450) inhibition studies (CYP2D6, CYP2C9, CYP3A4/5) were carried out
180 with pooled human liver microsomes using the conditions described in (21). Metabolite
181 identification was performed by LC-MS/MS, as described in (22), with a Phenomenex

Kinetex PFP column, 2.1 mm x 100 mm, 2.6 µm particles using microsomal incubations, incubations in hepatocytes from the hepatocyte stability assay, and *in vivo* mouse PK samples.

Plasma stability and whole blood-to-plasma partitioning ratio (B:P) were determined by spiking blood from humans (Australian Red Cross Blood bank), dogs, rats, or mice with UCT943 and incubating for 4 h at 37°C. During the incubation period, aliquots of blood were taken to confirm stability. At the end of the incubation period, duplicate aliquots of blood were taken and the remaining sample was centrifuged to collect duplicate aliquots of plasma. Concentrations in blood and the plasma fraction of blood were measured by LC-MS and the blood to plasma concentration ratio calculated using the mean concentration for each matrix.

2.5 Ethics statement

Animal experiments were approved by the institutional animal care and use committees for each of the experimental sites. All studies were conducted according to the appropriate legislation and respective institutional policies on animal use and welfare.

The human biological samples were sourced ethically and their research use was in accord with the terms of the informed consents.

2.6 Pharmacokinetic studies

Pharmacokinetic studies were performed in mice, rats, dogs and monkeys as described in the Supplementary Material. For comparison of blood clearance (CL_b) to hepatic blood flow, values of 90, 55, 31, 44, and 21 mL/min/kg were assumed in mice, rats, dogs, monkeys, and humans, respectively (23).

2.7 *In vivo* efficacy studies

In vivo efficacy studies were conducted in the *P. berghei* and in the *P. falciparum* NOD-*scid* *IL-2Rγ*^{null} (NSG) model as described previously (6, 24) (see Supplementary Material).

2.8 Prediction of human pharmacokinetics and efficacious single dose by pharmacokinetic/pharmacodynamic (PK/PD) modeling

2.8.1 Allometric scaling

The calculation of human plasma clearance (CL_p) and human plasma volume of distribution at steady state (V_{ss}) for UCT943 was carried out by a hybrid approach to allometric inter-species scaling (mouse, rat, dog, and monkey) of *in vivo* plasma CL_p and V_{ss} (25). After logarithmic/logarithmic transformation, the parameters were fitted to the equation log y = log a +b log BW, where BW is body weight; a and b are the allometric coefficient and exponent, respectively. Body weights of 0.025; 0.3; 5; 10 and 70 kg were used for mice, rats, monkeys, dogs, and humans, respectively. The mean residence time (MRT) was calculated from the predicted human plasma V_{ss} divided by the predicted human plasma CL_p.

2.8.2 PK/PD analysis in the Pf-infected NSG mouse model to predict minimum parasiticidal concentration (MPC)

Blood PK data from *Pf*-infected NSG mice were first fitted to a one-compartment model with first-order absorption and elimination. The predicted PK profiles were used to run a direct effect (DE) PK/PD model using Phoenix WinNonlin® (Certara, Princeton, NJ) in order to determine the minimum parasiticidal concentration (MPC) of UCT943 (Supplementary Material Equation S1 and S2).

225 *2.8.3 Simulation of human PK profiles for human dose prediction*

226 Dog and monkey data were used to predict human PK, since higher species allow more
227 extensive blood sampling to explore blood or plasma concentration against time curves in
228 detail. Intravenous (IV) and oral (PO) time course profiles were normalized in PKSolver
229 (Excel) for preclinical species and Wajima-transformed (26). The absorption rate constant
230 (k_a), and the bioavailability (F) estimates were obtained from PKSolver using the Wajima-
231 transformed data. Human PO PK parameters were predicted in Berkeley Madonna
232 (University of California, Berkeley, CA) using the Wajima transformed PK data, the human PK
233 parameters obtained from allometry in section 2.8.1, and the Ka and F estimates, to have
234 drug concentration above the MPC for ≥ 8 days. The single dose required to maintain the
235 human plasma concentration above the MPC for eight days (section 2.8.2) was determined
236 through simulation using the human PO PK profiles with Berkeley Madonna.

237 ## 2.9 *In vitro* cytotoxicity, cardiotoxicity and genotoxicity

238 *2.9.1 Cytotoxicity*

239 *In vitro* cytotoxicity of UCT943 was tested against L6 cells using the Alamar Blue assay, and
240 against Chinese Hamster Ovarian (CHO), Vero, and HepG2 cells, using the 3-(4,5-
241 dimethylthiazol-2-yl)-2,5-diphenyltetrazoliumbromide (MTT) assay (27, 28).

242 *2.9.2 Cardiotoxicity*

243 UCT943 was tested for inhibition of the human ether a go-go related gene (hERG) K^+ channel
244 ($K_v11.1$), human $K_v1.5$ K^+ channel, and human voltage-gated sodium channel $Na_v1.5$ using
245 IonWorks patch clamp electrophysiology (29), and for inhibition of the human $Ca_v1.2$
246 calcium channel (cardiac L-type) using a fluorescence Ca^{2+} assay. For all assays, 50%

cytotoxic concentrations (CC_{50}) were determined from 8-point dose-response curves generated using 3-fold serial dilutions from the maximum final assay concentration.

2.9.3 Genotoxicity

2.9.3.1 Ames

UCT943 was assessed for mutagenic toxicity by measuring its ability to induce reverse mutations in the *Salmonella typhimurium-Escherichia coli/*microsome plate incorporation assay (30, 31). Maximum concentrations were 5000 µg per plate.

2.9.3.2 Micronucleus

UCT943 capability to induce clastogenicity/aneugenicity in CHO-WBL cells was determined by measuring the extent of micronucleus formation with and without exogenous metabolic activation (Aroclor 1254 induced rat liver S9). Maximum concentrations were 500 µg/mL.

2.10 *In vivo* glucose-6-phosphate dehydrogenase (G6PD)-hemolysis

In vivo hemolytic toxicity was assessed in NOD-scid mice engrafted with A- G6PD-deficient human red blood cells (huRBCs) as described in (32) following 4-day treatment regimen at 1.5 and 10 mg/kg/day dose levels given orally.

3 RESULTS AND DISCUSSION

3.1 Rationale for optimization of MMV048 resulting in UCT943

Although MMV048 showed good potency against asexual blood stage parasites, there was room for improvement with respect to activity against liver and the transmissible gametocyte stage parasites(4).

During First-In-Human (FIH) studies, MMV048 showed high variability in exposure, which was attributed to low solubility. Intensive and time consuming formulation work had to be

carried out in order to identify a new formulation with a more consistent and 3-fold greater exposure (www.mmv.org/newsroom/interviews/mmv048-0).

To avoid such developability issues in future, improved solubility, pH-dependent and in biorelevant media, was identified as the main differentiating factor in follow-on compounds. Thus chemical modifications to MMV048 were made in such a way as to incorporate solubility-enhancing moieties. In this regard, the methyl sulfonyl group of MMV048 was replaced by a water solubilizing piperazinyl carboxamide on the phenyl ring at the 5-position of the 2-aminopyrazine core to deliver UCT943 (6). Improvements in asexual blood stage and liver stage activities were achieved by replacing the 2-aminopyridine ring with a 2-aminopyrazine ring, which also maintained good potency against gametocytes (6). One key objective of this study was firstly to determine if these improvements would translate into better in vivo efficacy in the *Pf*-infected NSG mouse model and accordingly, a low predicated human dose.

3.2 *In vitro* antiplasmodial activity

The biological target of the clinical candidate MMV048 was identified to be *Plasmodium* phosphatidylinositol 4-kinase (PI4K) through resistant mutant generation, sequencing, and pull-down experiments (4). *Plasmodium* PI4K has recently been identified as a new and promising drug target, which is present at all life-cycle stages of the *Pf* and *Pv* parasites (5). UCT943 inhibits the *Pv*PI4K enzyme with an IC_{50} = 23 nM. When tested against a 5-fold resistant *P. falciparum* strain generated against MMV048 due to the mutated *pfpi4k* locus (4), UCT943 displayed a 6-fold shift in IC_{50} relative to the parental Dd2 strain (14 nM relative to 2.2 nM) (Supplementary Material Table S2). When resistance was selected for in Dd2-B2 using UCT943, *pfpi4k* mutants with a 4- or 8-fold IC_{50} shift were obtained (Supplementary

292 Material Table S3). These mutants carried the G1309V or Y1342F mutations respectively,
293 and are located in the same region of *pi4k* as MMV048-selected mutations reported
294 elsewhere (4). Resistance selection studies indicated a minimum required inoculum of 10^7
295 Dd2 parasites for resistance to emerge, which is similar to MMV048 (4). By comparison, IC_{50}
296 shifts were within 2-fold when tested against strains containing mutated loci in either
297 *pfcytB*, *pfdhodh*, *pfatp4*, or *pfcarl.* These data indicate that UCT943 and MMV048 have the
298 same molecular target, and that similarly to MMV048, UCT943 is expected to have
299 transmission blocking and liver stage activity. Importantly, UCT943 maintained high *in vitro*
300 selectivity (> 200 fold) for the parasite *Pv*PI4K versus the human PI4KB isozyme (IC_{50} (PI4KB)
301 = 5.4 µM), which inhibition is linked to immunosuppressive effects (33).
302 UCT943 was one of the most potent compounds assessed in the 2-aminopyrazine chemical
303 series (6), with IC_{50}'s of 5.4 and 4.7 nM against NF54 and K1 *P. falciparum* strains,
304 respectively, which was 5- to 6-fold more active than the clinical candidate MMV048 (4)
305 (Figure 2). In addition, UCT943 was equally active against the drug sensitive NF54 strain and
306 multi-drug resistant strains, with IC_{50}'s ranging from 4 to 7 nM, thus suggesting that cross-
307 resistance with existing antimalarials is a low risk (Supplementary Material Table S1).
308 UCT943 primarily exhibited blood stage activity against schizonts (Supplementary Material
309 Table S5), which correlates with a slow rate of kill as determined in the *in vitro* parasite
310 reduction ratio (PRR) assay (lag phase = 48 h, Log PRR = 2.5 at 10 x EC_{50} in 3D7 strain) and in
311 the *in vitro* speed assay (Supplementary Material Table S5). As expected, the killing rate
312 profile of UCT943 was similar to that of MMV048 (lag phase = 48 h, Log PRR = 2.7) (4). When
313 tested against *Pf* clinical isolates of the Ivory Coast, UCT943 exhibited potent activity (2-15
314 nM) (Supplementary Material Table S6). The potency of UCT943 against clinical isolates

315 from Papua Indonesia was significantly higher than that of MMV048 in *Pv* and in *Pf* (median
316 IC_{50} 14 nM and 29 nM; p=0.012 versus median IC_{50} 93 nM and 202 nM; p<0.001) (Figure 2
317 and Supplementary Material Table S7). Interestingly, both compounds displayed higher
318 potency against *Pv* than *Pf*, a trend that was also observed for another PI4K inhibitor,
319 KDU691, albeit to a lesser extent (5).
320 When tested against other stages of the parasite life cycle (Figure 2), UCT943 was 2-50
321 times more potent than MMV048 (4). UCT943 was potent against early stage (>90% stage I-
322 III) and late stage gametocytes (>95% stage IV-V) (IC_{50} of 134 nM and 66 nM, respectively)
323 and inhibited the formation of both male and female gametes (IC_{50} ≈ 80 nM) in the dual
324 gamete formation assay (DGFA). The latter activity translated into transmission-blocking
325 activity (Target Candidate Profile TCP5 as defined by Burrows *et al.* (34)) in the standard
326 membrane feeding assay (SMFA), with an IC_{50} of 96 nM (35), equivalent to MMV048 (Figure
327 2) . In-depth clinical PK/PD investigations would be needed to determine doses that would
328 afford coverage for both blood stage and transmission-blocking activities. A single drug with
329 both activities would be a valuable addition to the arsenal of antimalarial medicines.
330 UCT943 also exhibits better *in vitro* liver stage activity than MMV048 (potentially addressing
331 TCP3 and TCP4 (34)), targeting schizonts *in vitro* (IC_{50} of < 100 nM and <10 nM in *P. vivax*
332 and *P. cynomolgi,* respectively, when tested prophylactically, and 0.92 nM in *P. berghei*), as
333 well as inhibiting the formation of hypnozoites (IC_{50} of < 100 nM and < 10 nM in *P. vivax* and
334 *P. cynomolgi,* respectively when tested prophylactically) (Figure 2). The parasitophorous
335 vacuole membrane protein UIS4 becomes internalized in MMV048-treated *P. berghei*
336 HepG2 cultures, a morphology associated with in vitro liver stage parasite clearance(4).

Though UCT943 was not evaluated for such morphological changes, its activity against schizonts offers prospects for improved prophylactic liver stage activity relative to MMV048.

3.3 Physicochemical characterization

UCT943 was stable in the solid state over a period of 18 months and was chemically stable at 20°C in solutions of DMSO, water (pH 6.2), and buffers (pH 2, pH 7.4) over 6 days. The piperazinylamide group accounts for the significantly lower measured lipophilicity of UCT943 (LogD = -0.27) relative to MMV048 (LogD = 2.6). This, combined with a pKa of 7.5, results in higher measured solubility in aqueous media compared to MMV048, across a range of physiologically relevant pH's up to 6.5, where the compound is protonated (Table 1). The compound was also highly soluble in SGF (pH 1.8), FeSSIF (pH 5.0), and FaSSIF media (pH 6.5) (> 1.5 mg/mL), predictive of a good dissolution in the gastrointestinal tract. The pH-dependent solubility profile of UCT943 in aqueous media was typical of a weak base with higher solubility at pH below the pKa, *i.e.* 7.5 (Figure 3). UCT943 exhibited high permeability across Caco-2 cells in both directions ($P_{app\ B>A}$ = 25 x 10^{-6} cm/s; $P_{app\ A>B}$ = 28 x 10^{-6} cm/s) without appreciable efflux (efflux ratio of 0.93, Table 2). With high FaSSIF solubility and high permeability, UCT943 could be classified as a Developability Classification System (DCS) Class I compound, which bodes well for a much more favorable development pathway compared to MMV048 that was classified as DCS Class II (Figure 4) (36). The high solubility and permeability of UCT943, along with its potent anti-*Plasmodium* activity against all stages of the parasite lifecycle (see section 3.1) triggered comprehensive DMPK profiling toward determining its potential for preclinical development.

3.4 *In vitro* and *in vivo* metabolism studies

There was no evidence of chemical instability for UCT943 in human, dog, rat, or mouse blood or plasma. The compound was moderately bound to plasma proteins with little species differentiation (f_u in plasma 0.10-0.16). It also had a greater propensity than MMV048 (B:P ~1.0 across species) to bind or distribute in red blood cells (RBCs) relative to plasma (B:P varying from 1.5 to 2.3 across species). This is likely due to enhanced partitioning through the acidic phospholipid bilayer of the cell membrane due to the weakly basic piperazine moiety. The higher partitioning into RBCs possibly contributes to a small degree to its potent *in vitro* and *in vivo* anti-*Plasmodium* activity by localizing the drug where the parasite resides.

As an indicator of hepatic metabolism, UCT943 was incubated across species with hepatocytes, liver microsomes, and liver S9 fraction (Table 2). The intrinsic clearance of UCT943 in both microsomes and hepatocytes was low in human, rat, and mouse (CL_{int} < 11.6 µL/min/mg in microsomes and CL_{int} < 4 µL/min/10^6 cells in hepatocytes), while it was moderate in dog (CL_{int} = 28.2 µL/min/mg in microsomes and CL_{int} = 9 µL/min/10^6 cells in hepatocytes). Additionally, no significant metabolism (< 10% degradation) was detected in human liver S9 fraction, showing that enzymes other than cytochrome P450s (CYPs) were not extensively involved in the metabolism of UCT943. No measurable inhibition was detected at 20 µM against any of the CYP isoforms tested (CYP2D6, CYP2C9, CYP3A4/5), indicating that UCT943 has low potential for *in vivo* enzyme inhibition and that adverse drug-drug interactions through oxidative metabolism are likely to be minimal.

Metabolite identification was performed *in vitro* using liver microsomes and hepatocytes, as well as *in vivo* by analyzing the collected blood samples from mouse PK experiments (Figure

5a). *In vitro*, liver microsomes and hepatocytes gave a complementary picture, both showing the major biotransformation pathway occurring on the piperazinylamide moiety (Figure 5b). UCT943 was mainly metabolized into an oxidation metabolite (P+16), which was further dehydrogenated into two metabolites P+14 (I&II) in non-human species. Further biotransformation on the piperazine ring gave metabolites P-26 (piperazine ring cleavage) and P+28. The formation of the carboxylic acid derivative by hydrolysis of the piperazinylamide moiety (P-68) was more easily detected in hepatocytes and *in vivo* in mice than in liver microsomes, presumably due to the higher concentration of the enzymes responsible for this particular biotransformation. The contribution of these metabolites to the activity of the parent UCT943 is currently under investigation. Notably, the P-68 metabolite, resulting from the hydrolysis of the carboxamide, showed high activity, albeit lower than that of the parent, with IC_{50}'s of 33 nM and 32 nM against *P. falciparum* NF54 and K1 strains respectively (6).

3.5 Pharmacokinetic studies

When administered intravenously, the blood clearance (CL_b) of UCT943 was low in mice, rats, and dogs (Table 3), with a value of less than 20% of hepatic blood flow (23) to very low in monkeys with blood CL < 5% hepatic blood flow, which is consistent with the high *in vitro* metabolic stability. Plasma volume of distribution was high in all species (V_{ss} 7.1 - 13.1 L/kg), suggesting that the compound extensively distributes and accumulates in organ tissues. This would be expected for a basic compound due to partitioning into cell membranes by associating with acidic phospholipids (37). As a consequence of the low CL and high V_{ss}, half-lives were long, ranging from 6 h in mice to 29 h in monkeys. When dosed orally in mice and dogs, UCT943 was rapidly absorbed (time of maximum concentration T_{max} < 3 h), while

absorption in rats and monkeys was slower with a maximum concentration (C_{max}) reached after 12 h and 7 h, respectively (Figure 6). Oral bioavailability was high across all species, ranging from 66% to 98%. The good oral bioavailability and the long $t_{1/2}$ of UCT943 across species is encouraging toward achieving a single dose treatment and cure for malaria, which would boost patient compliance in resource-limited regions of the world, where the medical infrastructure is not sufficient. If these PK properties are confirmed in humans, UCT943 could thus be a potential combination partner in a single exposure radical cure and prophylaxis (SERCaP) treatment as proposed by the Medicines for Malaria Venture (MMV) (34).

3.6 *In vivo* efficacy studies

When dosed at 10 mg/kg p.o., UCT943 reduced parasitemia by > 99.9% in the mouse *P. berghei* infection model and cured all mice with > 30 mean survival days (MSD). At 3 mg/kg p.o., no complete cure was achieved and MSD was 10 days (6), albeit parasitemia was reduced by 99%. The resulting 90% effective dose (ED_{90}) was 1.0 mg/kg p.o. in the *P. berghei* infection model. In the *Pf*-infected NSG mouse model (Supplementary Material Figure S1), UCT943 was 2-fold more potent than MMV048 with a ED_{90} (90% effective dose) of 0.25 mg/kg compared to 0.57 mg/kg (4). PK data showed that the exposure of UCT943 was dose-dependent (6). As PK/PD relationships in the humanized NSG mouse model have been found to be predictive of the induced blood-stage malaria (IBSM) model in human volunteers (38), we used the NSG mouse efficacy data for human dose prediction (see next section 3.7).

3.7 Prediction of human pharmacokinetics and efficacious single dose by PKPD modeling

3.7.1 Allometric scaling

The slope used to predict plasma CL by allometric scaling was close to 0.75 (0.73), while the slope used to predict plasma V_{ss} was close to 1 (0.90), as expected for metabolic processes and volumes, respectively (39) (Figure 7). The predicted human plasma V_{ss} was moderately large (6.3 L/kg) and the predicted human plasma CL was low (0.20 L/h/kg) as shown in Table 4. When converted using the B:P ratio of 1.5, the predicted human blood clearance was 0.10 L/h/kg, *i.e.* less than 10% of liver blood flow (23). The predicted $t_{1/2}$ in humans was 27 h, which together with a long mean residence time of 32 h, suggests that the compound will be a long-duration antimalarial agent.

3.7.2 Estimation of minimum parasiticidal concentration (MPC) in blood in the Pf-infected NSG mouse model

From the PK/PD model (Supplementary Material Figure S2 and S3), the compound specific PD parameters EC_{50} and K_{kill} were estimated to be 3.7 ng/mL and 0.060 /h respectively. The MPC in blood (MPC_b), calculated using the EC_{50}, was 7.4 ng/mL in NSG mouse blood and 5.2 ng/mL in human blood (Table 4), after correction for *Pf*-infected NSG mouse and human B:P partitioning data (2.8 and 1.5, respectively). The MPC in plasma (MPC_p) used for human dose prediction was therefore 2.6 ng/mL. The *in vivo* parasite reduction ratio (PRR) of 48 h predicted by the PK/PD model (Log PRR = 1.25) correlated closely to the *in vitro* moderate killing profile (Log PRR = 2.5), confirming UCT943 as a slow acting antimalarial compound in this model.

445 *3.7.3 Prediction of human pharmacokinetic parameters and efficacious dose*

446 The human PK profiles modeled in Berkeley Madonna predicted a single human dose of 50-
447 80 mg, based on dog and monkey data, respectively, in order to maintain the plasma
448 concentrations above the predicted therapeutic level (that is, the plasma MPC_p of 2.6
449 ng/mL) for 8 days (*i.e.* four asexual parasite cycles) (Supplementary Material Figure S4 and
450 S5). In this model, a single administration of the efficacious dose to maintain plasma
451 concentrations above the MPC_P for 8 days resulted in an area under the curve (AUC) of
452 4213-8223 ng·h/mL, and a predicted C_{max} of 234-358 ng/mL, based on monkey and dog,
453 respectively. The low predicted dose is particularly encouraging, since it leaves a generous
454 margin for potential dose increases, in case the predicted value was underestimated, or
455 dose increase was deemed desirable to prevent the development of resistance or to ensure
456 activity against other malaria species (including *P. vivax*, see section 3.1).

457 **3.8** *In vitro* cytotoxicity, cardiotoxicity and genotoxicity

458 Cytotoxicity, assessed against four mammalian cell lines, was found to be low with a
459 selectivity index (SI) greater than 2200 relative to the IC_{50} in NF54 and greater than 170-fold
460 against the highest IC_{50} in *Pf* clinical isolates (Table 5). The SI is equivalent or greater than
461 that of MMV048. Relative to the predicted upper unbound C_{max} (0.13 µM) for the human
462 efficacious plasma exposure, a 90-fold margin is thereby predicted and is sufficiently high to
463 warrant progression into *in vivo* preclinical toxicology studies.

464 The safety margins over cardiotoxicity risk were largely improved compared to MMV048
465 (see selectivity indexes SI in Table 5). The hERG IC_{50} of 10 µM corresponds to an 80-fold
466 margin relative to the predicted therapeutic unbound C_{max} exposure for efficacy, which
467 indicates a low risk of QT interval prolongation at therapeutic exposures. The margins to

potential safety issues associated with potential off-target activities at other ion channels ($Na_V1.5$, $Ca_V1.2$, and $K_V1.5$) are even higher (Table 5).

Genotoxicity was evaluated using the Ames and mouse micronucleus tests, in which UCT943 tested negative at the highest concentrations (Table 5), suggesting that the compound does not have the potential to result in back-mutation of a defective gene to recover its function (Ames test) (30), and does not have the ability to induce the formation of micronuclei during cell division as a consequence of genetic damage (micronucleus assay)(40).

3.9 *In vivo* G6PD-hemolysis

In the search for new antimalarial compounds, it is essential to develop drugs which do not pose a red blood cell hemolysis risk to patients with G6PD deficiency (34). When assessed for *in vivo* hemolytic toxicity in NOD-scid mice engrafted with A- G6PD-deficient human red blood cells (huRBCs), UCT943 showed comparable day 7 huRBC levels as those treated with the vehicle control, these levels being significantly higher when compared against the positive control primaquine (25 mg/kg/day). This indicates that UCT943 does not induce hemolytic toxicity at neither 1.5 nor 10 mg/kg/day dosing (Supplementary Material Figure S6), which is higher than the ED_{90} of 0.25 mg/kg in the *P. falciparum* NSG model of infection. Assessment of other markers of hemolysis, including spleen weight and mouse reticulocyte levels, also supports that UCT943 did not induce hemolytic toxicity (Supplementary Material Figures S7a and S7b).

4 CONCLUSION

UCT943 was optimized for antiplasmodial activity from a series of 2-aminopyrazines by structural modification of the clinical candidate MMV048, an inhibitor of an essential

490 *Plasmodium* enzyme, PI4K. Incorporation of a piperazinylamide group resulted in enhanced
491 water solubility while maintaining high permeability, both parameters being key for a good
492 developability profile and for achieving high drug exposure. This, combined with minimal *in*
493 *vitro* metabolism in liver subcellular fractions and in hepatocytes, translated into low
494 clearance, sustained exposure, and high bioavailability in preclinical species. UCT943 was
495 potent against all stages of the *Plasmodium* parasite lifecycle, as well as against resistant *P.*
496 *falciparum* and *P. vivax* clinical isolates. The 5-fold better *in vitro* antiplasmodial activity of
497 UCT943 compared to MMV048 translated into excellent efficacy in the *P. berghei* mouse
498 model and improved efficacy in the humanized *P. falciparum* mouse model. UCT943 was
499 found to be a slow acting, long duration antimalarial compound similar to what is seen for
500 quinoline antimalarials such as mefloquine. The predicted human single dose using monkey
501 and dog pharmacokinetics was low, ranging from 50 to 80 mg, which offers considerable
502 potential for the drug candidate. The high safety margins over cytotoxicity and cardiac
503 toxicity highlighted herein are much larger than the predicted human therapeutic exposure,
504 which is promising. Based on the data presented, UCT943 displays asexual blood stage,
505 transmission-blocking, and liver stage activity and thus has the potential to form part of a
506 single-exposure radical cure and prophylaxis (SERCaP) treatment of uncomplicated malaria.
507 This breadth of activity offers considerable flexibility with respect to treatment options and
508 TPPs that might be addressed and have contributed to the selection of UCT943 for
509 preclinical development as a follow-on compound to MMV048.
510
511 **Acknowledgments:** This paper is dedicated to S.M. Solapur. The authors would like to
512 acknowledge Nesia Barnes and Warren Olifant from H3D, University of Cape Town (South

513 Africa) for the ADME assays; Virgil Verhoog and Sumaya Salie from H3D, University of Cape
514 Town (South Africa) for the *Pf* blood stage assays; Trevor Finch from the Division of
515 Pharmacology, University of Cape Town (South Africa) for assistance with the animal work;
516 Michael Delves, Andrea Ruecker and Robert E. Sinden from the Cell and Molecular Biology
517 laboratory, Imperial College, London (United Kingdom) for the gamete formation assay;
518 Anne-Marie Zeeman and Clemens H. M Kocken from the Biomedical Primate Research
519 Centre, Rijswijk (The Netherlands) for the *Pc in vitro* prophylactic and radical cure assay;
520 Rachaneeporn Jenwithisuk from the Faculty of Tropical Medicine, Mahidol University,
521 Bangkok (Thailand) for the *Pv in vitro* prophylactic and radical cure assay; John Burke from
522 the University of Victoria, British Columbia (Canada) for the *Pv*PI4K assay.
523
524 **Funding:** We acknowledge the Medicines for Malaria Venture (project MMV09/0002),
525 Technology Innovation Agency (TIA) and the Strategic Health Innovation Partnerships (SHIP)
526 unit of the South African Medical Research Council (SAMRC) for financial support of this
527 research. K.C. acknowledges support from the University of Cape Town, SAMRC and South
528 African Research Chairs Initiative of the Department of Science and Technology
529 administered through the National Research Foundation. L.B. and T.C also acknowledge
530 support of SHIP.

Antimicrobial Agents and Chemotherapy

Tables

Table 1: Physico-chemical properties of UCT943 compared to MMV048

Property (SD)		*UCT943*	*MMV048*
MW (g/mol)		427.4	393.4
LogD	pH 7.4	-0.27 *(0.01)*	2.6 *(0.03)*
pKa	measured	7.45 *(0.05)*	4.0 *(0.07)*
Thermodynamic solubility (µg/mL)*	pH 2.0	3000	740
	pH 4.0	49	-
	pH 6.0	110	4.2 (pH 6.5)
	pH 8.0	31	4.0 (pH 7.4)
	pH 10.0	8.3	-
	SGF (pH 1.8)	5900	-
	FaSSIF (pH 6.5)	1500	14.4
	FeSSIF (pH 5.0)	1900	28.3 (pH 5.8)

SGF: Simulated Gastric Fluid; FaSSIF: Fasted State Simulated Intestinal Fluid; FeSSIF: Fed

State Simulated Intestinal Fluid

* single determination

536 ***Table 2: In vitro metabolism, permeability, protein binding, blood:plasma ratio and***

537 ***plasma stability data for UCT943***

Parameter h/d/r/m (SD)	
Microsomal CL_{int} (µL/min/mg)	<11.6 *(0.1)* / 28.2 *(0.5)* / <11.6 *(0.2)* / <11.6 *(0.7)*
Hepatocyte CL_{int} (µL/min/10^6 cells)*	<2 / 9 / 4 / <4
Hepatocyte predicted E_H*	<0.2 / 0.65 / 0.23 / <0.2
Caco-2 $P_{app\ B>A}$ / $P_{app\ A>B}$ (10^{-6} cm/s)	25 *(5)* / 28 *(2)*
f_u microsomes	0.15 *(0.01)* / 0.50 *(0.04)* / 0.45 *(0.05)* / 0.47 *(0.04)*
f_u plasma	0.17 *(0.009)* / 0.10 *(0.007)* / 0.15 *(0.009)* / 0.10 *(0.02)*
Blood:Plasma ratio	1.5 *(0.1)* / 2.3 *(0.1)* / 2.1 *(0.2)* / 1.9 *(0.2)*
Plasma stability (% after 240 min)*	97 / 95 / 97 / 102

538 * single determination

Table 3: *In vivo* pharmacokinetic parameters for UCT943 across mouse, rat, dog, and monkey species calculated from non-compartmental analysis *(SD are given in brackets)*

Species	*Mouse*	*Mouse*	*Rat*	*Rat*	*Dog*	*Dog*	*Monkey*	*Monkey*
Dose (mg/kg)	5 (IV)	20 (PO)	5 (IV)	20 (PO)	2 (IV)	10 (PO)	2 (IV)	10 (PO)
$t_{1/2}$ (h)	6.4 *(0.7)*	5.7 *(0)*	7.4 *(0.6)*	5.3 *(0.3)*	13.0	16.1	28.6	34.6
Plasma V_{ss} (L/kg)	13.1* *(1.1)*	-	11.5**(2.1)*	-	7.1 *(0.9)*	-	8.7 *(1.0)*	-
Blood CL_b (mL/min/kg)	12.6 *(2.4)*	-	9.5 *(1.6)*	-	3.3* *(0.6)*	-	2.0 **(0.3)*	-
Plasma CL_p (mL/min/kg)	24.0* *(4.6)*	-	20.0**(3.4)*	-	7.5 *(1.2)*	-	3.9 *(0.6)*	-
Plasma $AUC_{0-\infty\ p}$ (min·µM)	497* *(8.5)*	1310**(202)*	725**(109)*	2843**(480)*	634 *(89)*	2335 *(754)*	1192 *(164)*	4745 *(761)*
Plasma C_{max} (µM)	1.2* *(0.2)*	1.7* *(0.3)*	2.4**(0.2)*	2.1**(0.7)*	1.0 *(0.1)*	2.3 *(0.4)*	1.5 *(0.03)*	2.1 *(0.4)*
T_{max} (h)	-	4.0 *(3.6)*	-	12.0	-	2.3 *(1.5)*	-	7.0 *(1.7)*
F (%)	-	66 *(10)*	-	98 *(4.9)*	-	74 *(23.7)*	-	80 *(12.8)*

*blood values were scaled to plasma values using B:P ratios of 1.9/2.1/2.3/2.0 for mice, rats, dogs, and monkeys, respectively

$_b$ blood; $_p$ plasma

544 ***Table 4: Predicted human PK parameters for UCT943 from modeling***

Parameter	*UCT943*
Plasma V_{ss} (L/kg)	6.3
Plasma CL_p (L/h/kg)	0.20
MRT (h)	32
Plasma MPC_p (ng/mL); blood MPC_b (ng/mL);	2.6; 5.2
k_a (/h)	0.25
F (%)	80
Single dose (mg)*	50-80
$t_{1/2}$ (h)	27
Plasma AUC_p (ng·h/mL)	4213-8223
Plasma $C_{max\ p}$ (ng/mL)	234-358

545 MPC: Minimum Parasiticidal Concentration

546 *Predicted single dose to achieve ≥8 days above MPC

547 $_b$ blood; $_p$ plasma

548 ***Table 5: Cytotoxicity, cardiotoxicity and genotoxicity data for UCT943 and MMV048***

		MMV048	*UCT943*	
	Cell line / Ion channel	CC_{50} µM (SI)	CC_{50} µM (SI)	Lowest SI
Cytotoxicity	CHO	-	17 (3148x)	298
	Vero	-	113 (20926x)	1982
	HepG2	>10 (357x)	13 (2407x)	225
	L6	251 (8964x)	12 (2222x)	211
Cardiotoxicity	hERG (K_V11.1)	>11 (393x)	10 [6.4-15.9] (1870x)	177
	Na_V1.5	100 (3571x)	>33 (>6111x)	>579
	Ca_V1.2	16 (571x)	>33 (>6111x)	>579
	K_V1.5	-	>33 (>6111x)	>579
Genotoxicity	Ames assay	Negative	Negative	-
	Micronucleus test	Negative	Negative	-

549 CC_{50}: 50% cytotoxic concentration

550 IC_{50}: 50% inhibitory concentration

551 SI: selectivity index; SI = CC_{50} / IC_{50} NF54 ;

552 Lowest SI; lowest selectivity index against clinical isolates; lowest SI = CC_{50} /max IC_{50} Pf

553 clinical isolate

554 Figures

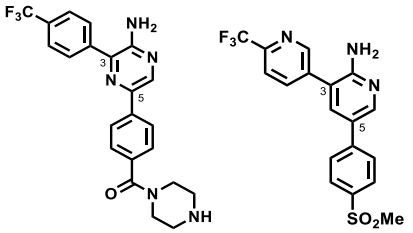

555

556 UCT943 MMV048

557 ***Figure 1 Structure of UCT943 and MMV048***

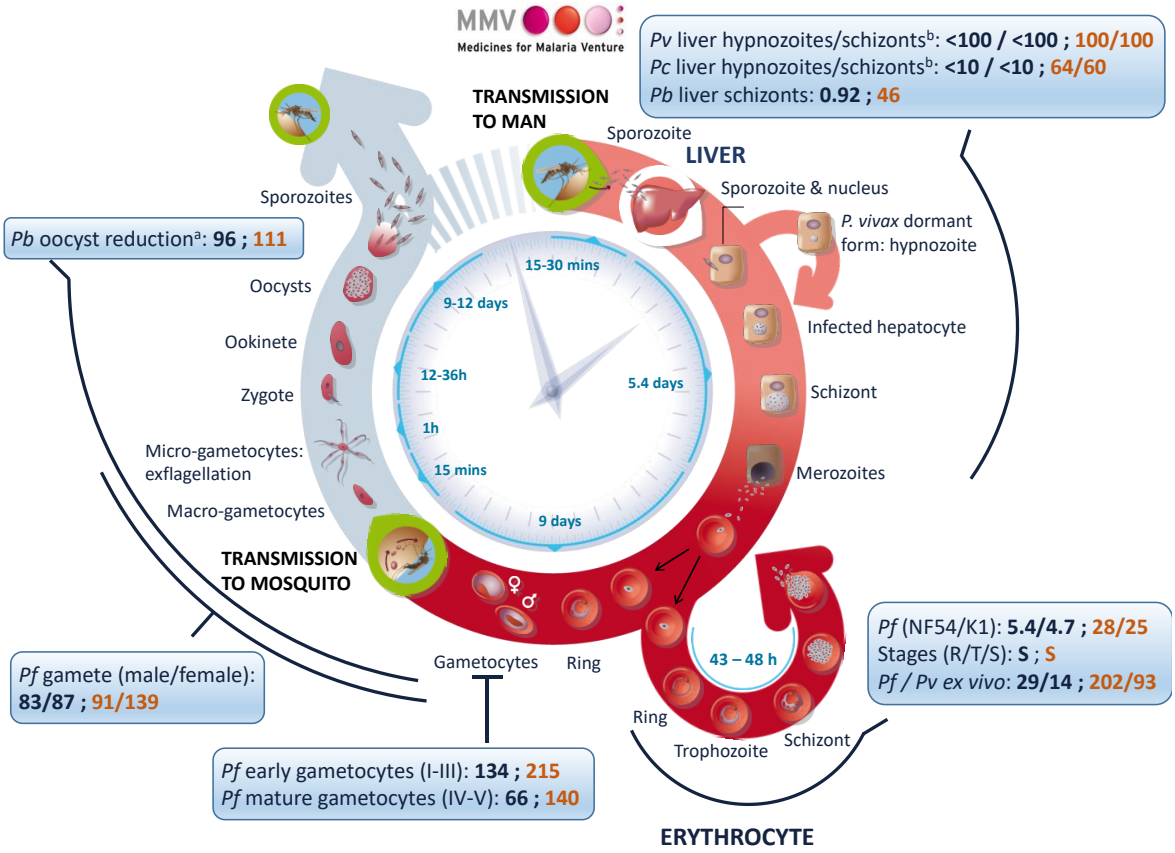

558

559 ***Figure 2: Antiplasmodial activity of UCT943 compared to MMV048 against different stages***

560 ***of the parasite life cycle (values indicate IC_{50} in nM; blue: UCT943; brown: MMV048)***

561 [a] Standard Membrane Feeding Assay, indirect mode (35)

562 [b] prophylactic assay

Antimicrobial Agents and Chemotherapy

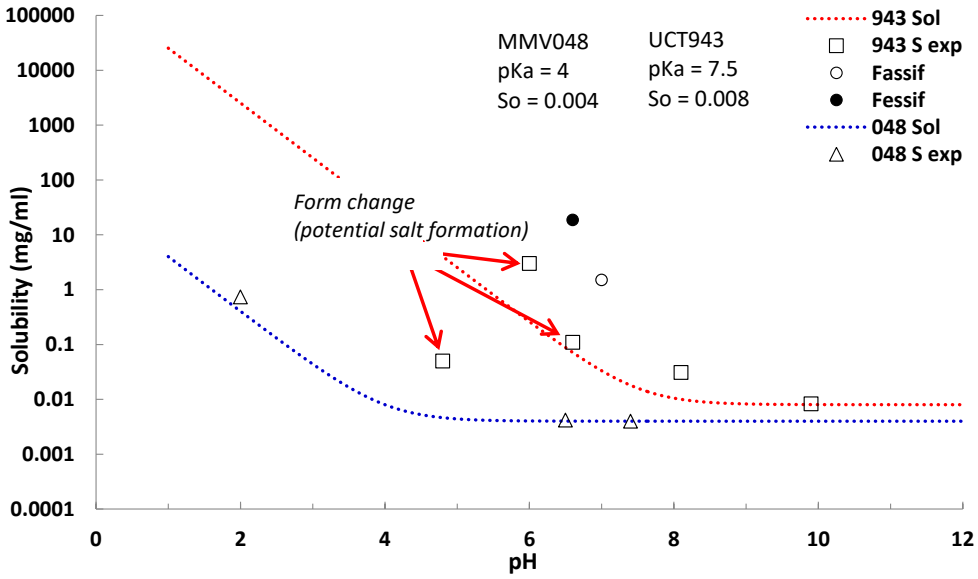

563

564 ***Figure 3: Comparison of pH solubility profiles of MMV048 (dotted blue line) and UCT943***

565 ***(dotted red line) calculated and measured values for MMV048 (triangle dots), and UCT943***

566 ***(square dots)***

567 FaSSIF: Fasted State Simulated Intestinal Fluid; FeSSIF: Fed State Simulated Intestinal Fluid

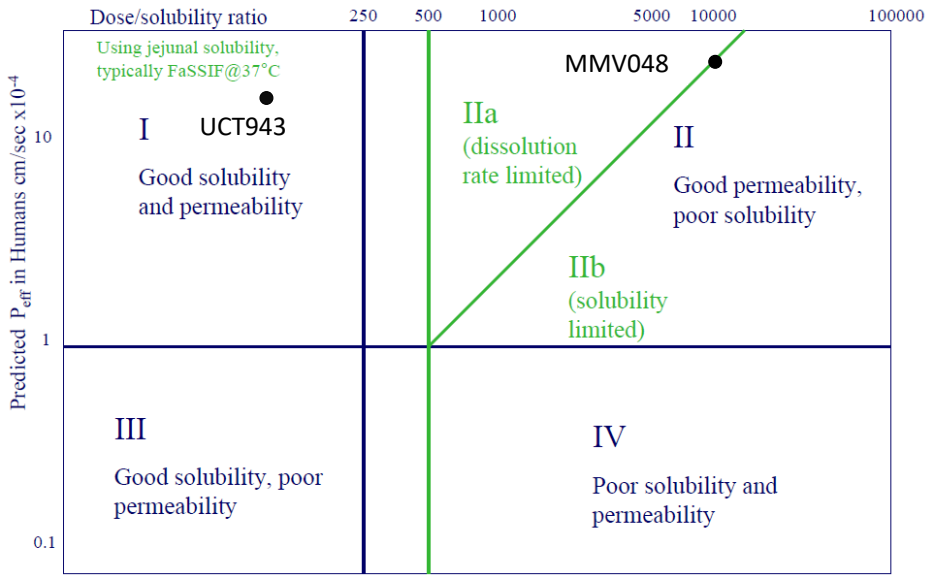

568

569 ***Figure 4: Ranking of UCT943 and MMV048 in the Developability Classification System***

570 ***(DCS) (36).***

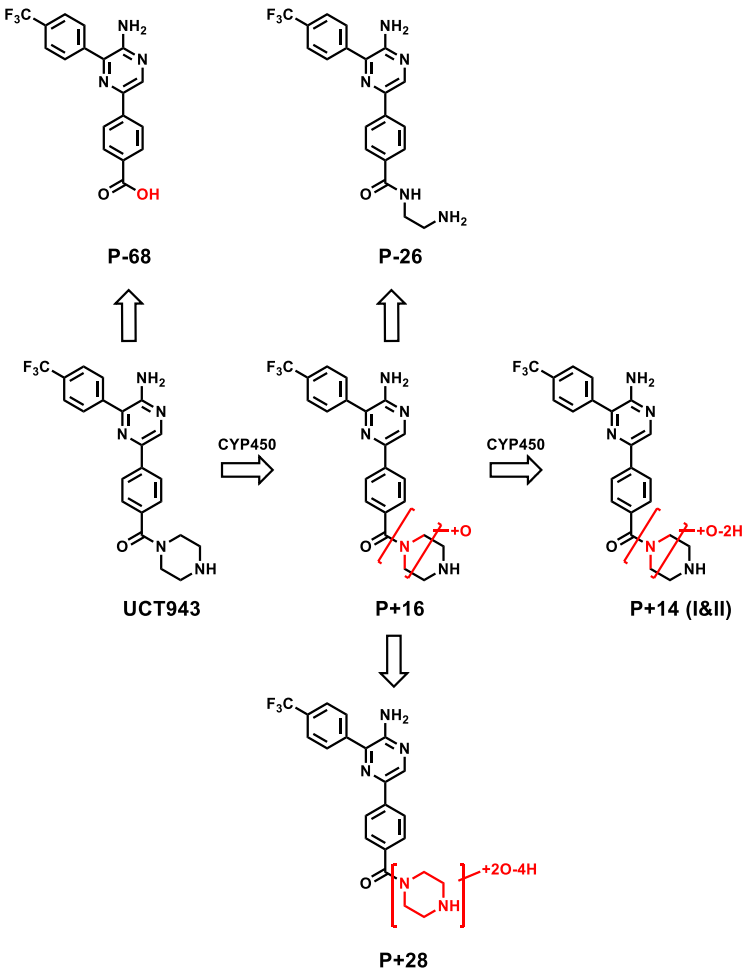

571

572 ***Figure 5a: Proposed metabolic pathway of UCT943 in microsomes (mouse, rat, human),***

573 ***hepatocytes and in vivo in mice***

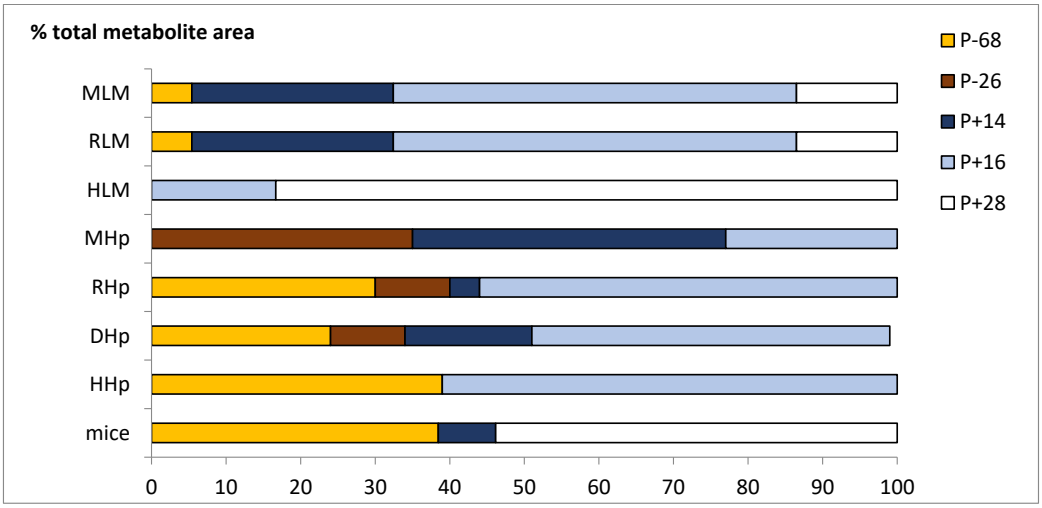

574

575 ***Figure 5b: Metabolite profiles of UCT943 in liver microsomes, hepatocytes, and in mice***

576 LM: liver microsomes; Hp: hepatocytes; H: human; R: rat; M: mice; D: dog

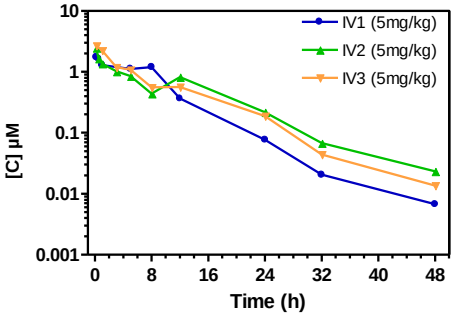

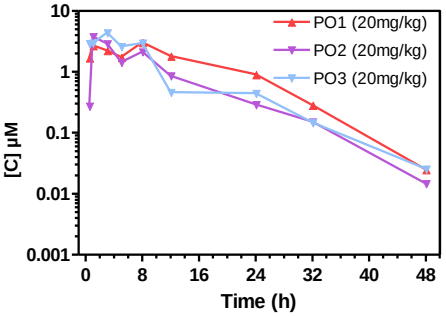

577

578 (a) (b)

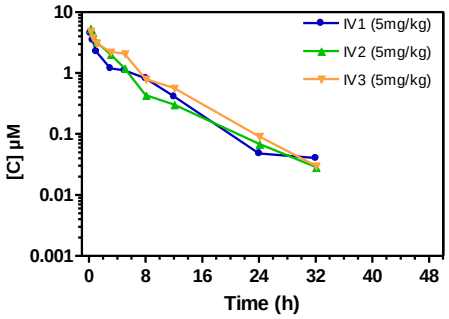

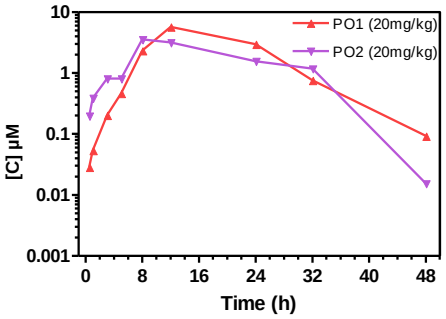

579

580 (c) (d)

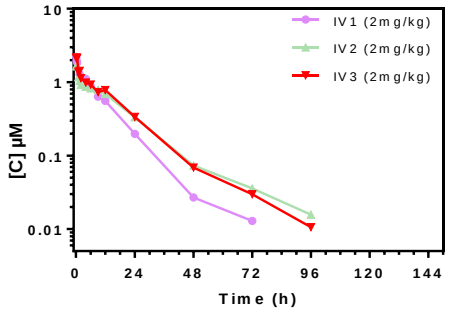

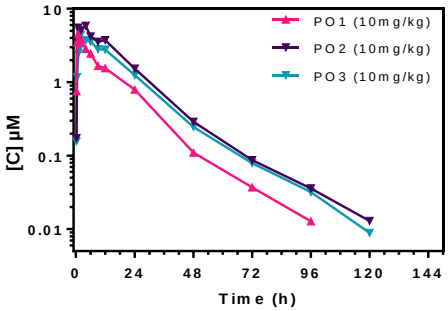

581
582 (e) (f)

Antimicrobial Agents and Chemotherapy

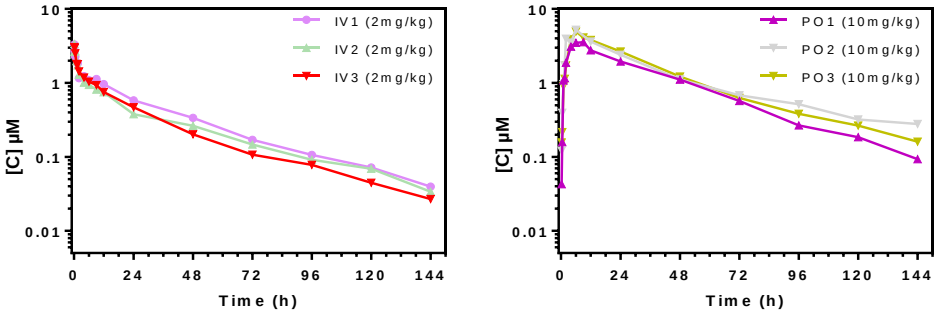

583
584 (g) (h)

585 ***Figure 6: Whole blood concentration vs time profiles following IV (left) and oral (right)***

586 ***administration of UCT943 to (a, b) non-fasted male Balb/C mice; (c, d) fasted male***

587 ***Sprague Dawley rats; (e, f) fasted male beagle dogs; (g, h) fasted female Cynomolgus***

588 ***monkeys***

589

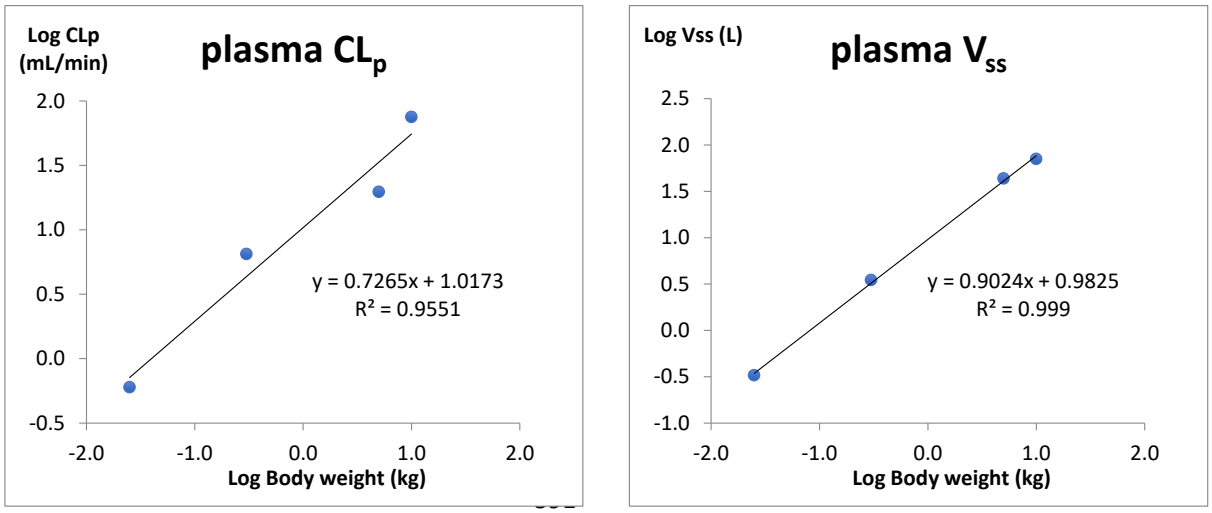

590

592 (a) (b)

593 ***Figure 7: Allometric plot for UCT943 (a) plasma clearance and (b) plasma volume of***

594 ***distribution***

595 References

1. WHO (World Health Organisation). 2017. World malaria report 2017, 160p.
2. Takala-Harrison S, Laufer MK. 2015. Antimalarial drug resistance in Africa: key lessons for the future. Ann N Y Acad Sci 1342:62–67.
3. Mbengue A, Bhattacharjee S, Pandharkar T, Liu H, Estiu G, Stahelin R V., Njimoh DL, Ryan Y, Chotivanich K, Nguon C, Ghorbal M, Lopez-Rubio JJ, Pfrender M, Emrich S, Mohandas N, Dondorp AM, Wiest O, Haldar K. 2015. A molecular mechanism of artemisinin resistance in *Plasmodium falciparum* malaria. Nature 520:683–687.
4. Paquet T, Le Manach C, González Cabrera D, Younis Y, Henrich PP, Abraham TS, Lee MCS, Basak R, Ghidelli-Disse S, Lafuente-Monasterio MJ, Bantscheff M, Ruecker A, Blagborough AM, Zakutansky SE, Zeeman A-M, White KL, Shackleford DM, Mannila J, Morizzi J, Scheurer C, Angulo-Barturen I, Santos-Martínez M, Ferrer S, Sanz LM, Gamo FJ, Reader J, Botha MJ, Dechering KJ, Sauerwein RW, Tungtaeng A, Vanachayangkul P, Lim CS, Burrows JN, Witty MJ, Marsh KC, Bodenreider C, Rochford R, Solapure SM, Jiménez-Díaz MB, Wittlin S, Charman SA, Donini C, Campo B, Birkholtz L-M, Hanson KK, Drewes G, Kocken CHM, Delves MJ, Leroy D, Fidock DA, Waterson D, Street LJ, Chibale K. 2017. Antimalarial efficacy of MMV390048, an inhibitor of *Plasmodium* phosphatidylinositol 4-kinase. Sci Transl Med 9:eaad9735.
5. McNamara CW, Lee MCS, Lim CS, Lim SH, Roland J, Nagle A, Simon O, Yeung BKS, Chatterjee AK, McCormack SL, Manary MJ, Zeeman A-M, Dechering KJ, Kumar TRS, Henrich PP, Gagaring K, Ibanez M, Kato N, Kuhen KL, Fischli C, Rottmann M, Plouffe DM, Bursulaya B, Meister S, Rameh L, Trappe J, Haasen D, Timmerman M, Sauerwein RW, Suwanarusk R, Russell B, Renia L, Nosten F, Tully DC, Kocken CHM, Glynne RJ, Bodenreider C, Fidock DA, Diagana TT, Winzeler EA. 2013. Targeting *Plasmodium*

PI(4)K to eliminate malaria. Nature 504:248–253.

6. Le Manach C, Nchinda AT, Paquet T, Gonzalez Cabrera D, Younis Y, Han Z, Bashyam S, Zabiulla M, Taylor D, Lawrence N, White KL, Charman SA, Waterson D, Witty MJ, Wittlin S, Botha ME, Nondaba SH, Reader J, Birkholtz L-M, Jimenez-Diaz M-B, Santos Martinez M, Ferrer S, Angulo-Barturen I, Meister S, Antonova-Koch Y, Winzeler EA, Street LJ, Chibale K. 2016. Identification of a potential antimalarial drug candidate from a series of 2-aminopyrazines by optimization of aqueous solubility and potency across the parasite life cycle. J Med Chem 59:9890–9905.

7. Desjardins RE, Canfield CJ, Haynes JD, Chulay JD. 1979. Quantitative assessment of antimalarial activity *in vitro* by a semiautomated dilution technique. Antimicrob Agents Chemother 16:710–718.

8. Matile H, Pink JRL. 1990. *Plasmodium falciparum* malaria parasite cultures and their use in immunology, p. 221–234. *In* Lefkovits, I. & Pernis, B., E (ed.), Immunological Methods. Academic Press, San Diego, CA, USA.

9. Phillips MA, White KL, Kokkonda S, Deng X, White J, El Mazouni F, Marsh K, Tomchick DR, Manjalanagara K, Rudra KR, Wirjanata G, Noviyanti R, Price RN, Marfurt J, Shackleford DM, Chiu FCK, Campbell M, Jimenez-Diaz MB, Bazaga SF, Angulo-Barturen I, Martinez MS, Lafuente-Monasterio M, Kaminsky W, Silue K, Zeeman A-M, Kocken C, Leroy D, Blasco B, Rossignol E, Rueckle T, Matthews D, Burrows JN, Waterson D, Palmer MJ, Rathod PK, Charman SA. 2016. A triazolopyrimidine-based dihydroorotate dehydrogenase inhibitor with improved drug-like properties for treatment and prevention of malaria. ACS Infect Dis 2:945–957.

10. Silvie O, Rubinstein E, Franetich J-F, Prenant M, Belnoue E, Rénia L, Hannoun L, Eling W, Levy S, Boucheix C, Mazier D. 2003. Hepatocyte CD81 is required for *Plasmodium*

falciparum and *Plasmodium yoelii* sporozoite infectivity. Nat Med 9:93–96.

11. Yalaoui S, Zougbédé S, Charrin S, Silvie O, Arduise C, Farhati K, Boucheix C, Mazier D, Rubinstein E, Froissard P. 2008. Hepatocyte permissiveness to *Plasmodium* infection is conveyed by a short and structurally conserved region of the CD81 large extracellular domain. PLoS Pathog 4:e1000010.

12. Zeeman AM, Van Amsterdam SM, McNamara CW, Voorberg-van Der Wel A, Klooster EJ, Van Den Berg A, Remarque EJ, Plouffe DM, Van Gemert GJ, Luty A, Sauerwein R, Gagaring K, Borboa R, Chen Z, Kuhen K, Glynne RJ, Chatterjee AK, Nagle A, Roland J, Winzeler EA, Leroy D, Campo B, Diagana TT, Yeung BKS, Thomas AW, Kocken CHM. 2014. KAI407, a potent non-8-aminoquinoline compound that kills *Plasmodium cynomolgi* early dormant liver stage parasites in vitro. Antimicrob Agents Chemother 58:1586–1595.

13. Sattabongkot J, Yimamnuaychoke N, Leelaudomlipi S, Rasameesoraj M, Jenwithisuk R, Coleman RE, Udomsangpetch R, Cui L, Brewer TG. 2006. Establishment of a human hepatocyte line that supports *in vitro* development of the exo-erythrocytic stages of the malaria parasites *Plasmodium falciparum* and *P. vivax*. Am J Trop Med Hyg 74:708–715.

14. Reader J, Botha M, Theron A, Lauterbach SB, Rossouw C, Engelbrecht D, Wepener M, Smit A, Leroy D, Mancama D, Coetzer TL, Birkholtz L-M. 2015. Nowhere to hide: interrogating different metabolic parameters of Plasmodium falciparum gametocytes in a transmission blocking drug discovery pipeline towards malaria elimination. Malar J 14:1–17.

15. Ruecker A, Mathias DK, Straschil U, Churcher TS, Dinglasan RR, Leroy D, Sinden RE, Delves MJ. 2014. A male and female gametocyte functional viability assay to identify

Antimicrobial Agents and Chemotherapy

biologically relevant malaria transmission-blocking drugs. Antimicrob Agents Chemother 58:7292–7304.

16. Baragaña B, Hallyburton I, Lee MCS, Norcross NR, Grimaldi R, Otto TD, Proto WR, Blagborough AM, Meister S, Wirjanata G, Ruecker A, Upton LM, Abraham TS, Almeida MJ, Pradhan A, Porzelle A, Martínez MS, Bolscher JM, Woodland A, Luksch T, Norval S, Zuccotto F, Thomas J, Simeons F, Stojanovski L, Osuna-Cabello M, Brock PM, Churcher TS, Sala KA, Zakutansky SE, Jiménez-Díaz MB, Sanz LM, Riley J, Basak R, Campbell M, Avery VM, Sauerwein RW, Dechering KJ, Noviyanti R, Campo B, Frearson JA, Angulo-Barturen I, Ferrer-Bazaga S, Gamo FJ, Wyatt PG, Leroy D, Siegl P, Delves MJ, Kyle DE, Wittlin S, Marfurt J, Price RN, Sinden RE, Winzeler EA, Charman SA, Bebrevska L, Gray DW, Campbell S, Fairlamb AH, Willis PA, Rayner JC, Fidock DA, Read KD, Gilbert IH. 2015. A novel multiple-stage antimalarial agent that inhibits protein synthesis. Nature 522:315–320.

17. Gibhard L, Pravin K, Abay E, Wilhelm A, Swart K, Lawrence N, Khoury R, van der Westhuizen J, Smith P, Lubbe Wiesner. 2016. *In Vitro* and *in vivo* pharmacokinetics of aminoalkylated diarylpropanes NP085 and NP102. Antimicrob Agents Chemother 60:3065–3069.

18. Phillips MA, Lotharius J, Marsh K, White J, Dayan A, White KL, Njoroge JW, Mazouni F El, Lao Y, Kokkonda S, Tomchick DR, Deng X, Laird T, Bhatia SN, March S, Ng CL, Fidock DA, Wittlin S, Lafuente-Monasterio M, Gamo Benito JF, Sanz Alonso LM, Santos Martinez M, Jimenez-Diaz, Maria Belen Ferrer Bazaga S, Angulo-Barturen I, Haselden JN, Louttit J, Cui Y, Sridhar A, Zeeman A-M, Kocken C, Sauerwein R, Dechering K, Avery VM, Duffy S, Delves M, Sinden R, Ruecker A, Wickham, Kristina S. Rochford R, Gahagen J, Iyer L, Riccio E, Mirsalis J, Bathhurst I, Rueckle T, Ding X,

Campo B, Leroy D, Rogers MJ, Rathod PK, Burrows JN, Charman SA. 2015. A long-duration dihydroorotate dehydrogenase inhibitor (DSM265) for prevention and treatment of malaria. Sci Transl Med 7:296ra111.

19. Ring BJ, Chien JY, Adkison KK, Jones HM, Rowland M, Jones R Do, Yates JWT, Ku MS, Gibson CR, He H, Vuppugalla R, Marathe P, Fischer V, Dutta S, Sinha VK, Björnsson T, Lavé T, Poulin P. 2011. PhRMA CPCDC initiative on predictive models of human pharmacokinetics, part 3: Comparative assessement of prediction methods of human clearance. J Pharm Sci 100:4090–4110.

20. Coteron JM, Marco M, Esquivias J, Deng X, White KL, White J, Koltun M, El Mazouni F, Kokkonda S, Katneni K, Bhamidipati R, Shackleford DM, Angulo-Barturen I, Ferrer SB, Jiménez-Díaz MB, Gamo F-J, Goldsmith EJ, Charman WN, Bathurst I, Floyd D, Matthews D, Burrows JN, Rathod PK, Charman SA, Phillips MA. 2011. Structure-guided lead optimization of triazolopyrimidine-ring substituents identifies potent *Plasmodium falciparum* dihydroorotate dehydrogenase inhibitors with clinical candidate potential. J Med Chem 54:5540–5561.

21. Walsky RL, Obach RS. 2004. Validated assays for human cytochrome P450 activities. Drug Metab Dispos 32:647–60.

22. Le Manach C, Paquet T, Brunschwig C, Njoroge M, Han Z, Gonzalez Cabrera D, Bashyam S, Dhinakaran R, Taylor D, Reader J, Botha M, Churchyard A, Lauterbach S, Coetzer T, Birkholtz L-M, Meister S, Winzeler EA, Waterson D, Witty MJ, Wittlin S, Jimenez-Diaz M-B, Santos Martinez M, Ferrer S, Angulo-Barturen I, Street LJ, Chibale K. 2015. A novel pyrazolopyridine with in vivo activity in *Plasmodium berghei*- and *Plasmodium falciparum*-infected mouse models from structure-activity relationship studies around the core of recently identified antimalarial imidazopyridazines. J Med

Chem 58:8713–8722.

23. Davies B, Morris T. 1993. Physiological parameters in laboratory animals and humans. Pharm Res 10:1093–1095.

24. Jiménez-Díaz MB, Mulet T, Viera S, Gómez V, Garuti H, Ibáñez J, Alvarez-Doval A, Shultz LD, Martínez A, Gargallo-Viola D, Angulo-Barturen I. 2009. Improved murine model of malaria using *Plasmodium falciparum* competent strains and non-myelodepleted NOD-*scid IL2Rγ*^{null} mice engrafted with human erythrocytes. Antimicrob Agents Chemother 53:4533–4536.

25. Boxenbaum H. 1982. Interspecies scaling, allometry, physiological time, and the ground plan of pharmacokinetics. J Pharmacokinet Biopharm 10:201–227.

26. Wajima T, Yano Y, Fukumura K, Oguma T. 2004. Prediction of human pharmacokinetic profile in animal scale up based on normalizing time course profiles. J Pharm Sci 93:1890–1900.

27. Mosmann T. 1983. Rapid colorimetric assay for cellular growth and survival: Application to proliferation and cytotoxicity assays. J Immunol Methods 65:55–63.

28. Rubinstein L V., Shoemaker RH, Paull KD, Simon RM, Tosini S, Skehan P, Scudiero DA, Monks A, Boyd MR. 1990. Comparison of *in vitro* anticancer-drug-screening data generated with a tetrazolium assay against a diverse panel of human tumor cell lines. J Natl Cancer Inst 82:1113–1118.

29. Schroeder K, Neagle B, Trezise DJ, Worley J. 2003. IonWorks (TM) HT: A new high-throughput electrophysiology measurement platform. J Biomol Screen 8:50–64.

30. Mortelmans K, Zeiger E. 2000. The Ames *Salmonella*/microsome mutagenicity assay. Mutat Res 455:29–60.

31. Mortelmans K, Riccio ES. 2000. The bacterial tryptophan reverse mutation assay with

Escherichia coli WP2. Mutat Res - Fundam Mol Mech Mutagen 455:61–69.

32. Rochford R, Ohrt C, Baresel PC, Campo B, Sampath A, Magill AJ, Tekwani BL, Walker LA. 2013. Humanized mouse model of glucose 6-phosphate dehydrogenase deficiency for *in vivo* assessment of hemolytic toxicity. Proc Natl Acad Sci U S A 110:17486–17491.

33. LaMarche MJ, Borawski J, Bose A, Capacci-Daniel C, Colvin R, Dennehy M, Ding J, Dobler M, Drumm J, Gaither LA, Gao J, Jiang X, Lin K, McKeever U, Puyang X, Raman P, Thohan S, Tommasi R, Wagner K, Xiong X, Zabawa T, Zhu S, Wiedmann B. 2012. Anti-hepatitis C virus activity and toxicity of type III phosphatidylinositol-4-kinase beta inhibitors. Antimicrob Agents Chemother 56:5149–5156.

34. Burrows JN, Duparc S, Gutteridge WE, van Huijsduijnen R, Kaszubska W, Macintyre F, Mazzuri S, Möhrle JJ, Wells TNC. 2017. New developments in anti-malarial target candidate and product profiles. Malar J 16:26.

35. Van der Watt M, Reader J, Churchyard A, Nondaba SH, Lauterbach SB, Niemand J, Abayomi S, Van Biljon RA, Connacher JI, Van Wyk RDJ, Le Manach C, Paquet T, Gonzalez Cabrera D, Brunschwig C, Theron A, Lozano-Arias S, Rodrigues JFI, Herreros E, Leroy D, Duffy J, Street LJ, Chibale K, Mancama D, Coetzer TL, Birkholtz L-M. 2018. Potent *Plasmodium falciparum* gametocytocidal compounds identified by exploring the kinase inhibitor chemical space for dual active antimalarials. J Antimicrob Chemother in press.

36. Butler JM, Dressman JB. 2010. The Developability Classification System : application of biopharmaceutics concepts to formulation development. J Pharm Sci 99:4940–4954.

37. Smith DA, Di L, Kerns EH. 2010. The effect of plasma protein binding on *in vivo*

efficacy: misconceptions in drug discovery. Nat Rev Drug Discov 9:929–939.

38. McCarthy JS, Marquart L, Sekuloski S, Trenholme K, Elliott S, Griffin P, Rockett R, O'Rourke P, Sloots T, Angulo-Barturen I, Ferrer S, Jiménez-Díaz MB, Santos Martinez M, Hooft van Huijsduijnen R, Duparc S, Leroy D, Wells TNC, Baker M, Möhrle JJ. 2016. Linking murine and human *Plasmodium falciparum* challenge models in a translational path for antimalarial drug development. Antimicrob Agents Chemother 60:3669–3675.

39. Anderson BJ, Holford NHG. 2008. Mechanism-based concepts of size and maturity in pharmacokinetics. Annu Rev Pharmacol Toxicol 48:303–332.

40. Corvi R, Albertini S, Hartung T, Hoffmann S, Maurici D, Pfuhler S, Van Benthem J, Vanparys P. 2008. ECVAM retrospective validation of *in vitro* micronucleus test (MNT). Mutagenesis 23:271–283.

596